THE JOURNAL OF PHYSICAL CHEMISTRY C

ARTICLE

pubs.acs.org/JPCC

Statistics on Surface-Enhanced Resonance Raman Scattering from Single Nanoshells

Celly M. S. Izumi, Matthew G. Moffitt, and Alexandre G. Brolo*

Department of Chemistry, University of Victoria, Post Office Box 3065, Victoria, British Columbia V8W 3V6, Canada

ABSTRACT: Silver nanoshells on polystyrene microspheres were used as substrates for surface-enhanced resonance Raman scattering (SERRS). SERRS mapping was recorded from isolated nanoshells coated with Nile blue (NB) and immobilized on gold films and silicon surfaces. Variations in the position and the shape of the ~590 cm^{-1} SERRS band of NB within a single nanoshell were observed, as well as fluctuations in integrated SERRS intensities between different isolated nanoshells. The frequency variations were assigned either to different adsorption sites or to different molecular adsorption geometries within a single nanoshell. The intensity fluctuations were rationalized by considering distinct distributions of electromagnetic hotspots in different nanoshells. The SERRS intensity distribution statistics presents a skewed shape with a long tail, which is similar to the characteristic Pareto distribution observed in "single-molecule" surface-enhanced Raman scattering (SERS). The data indicate that a small number of nanoshells yield integrated SERRS intensities an order of magnitude larger than the average, due to the presence of highly efficient hotspots. The statistics of nanoshell SERS presented here points to the need for rigorous analysis of inherent signal variability when such substrates are applied for single-particle chemical sensing and SERS imaging.

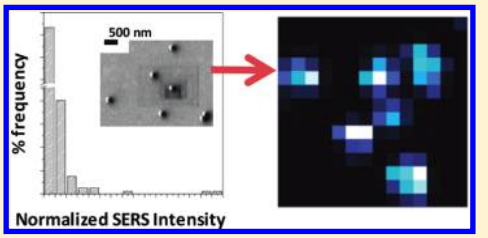

During the past four decades, surface-enhanced Raman scattering (SERS) has been used as a powerful tool for molecular characterization, electrochemistry, chemical sensing, and medical diagnostics. The SERS phenomenon occurs near nanostructured surfaces that sustain localized surface plasmon resonances.[1−7] Although silver or gold colloids are the traditional SERS substrates,[1,2] the development of SERS has been accompanied by a growing number of reports on the fabrication of new types of nanoparticles with controlled plasmonic properties.[4−13] Nanoshells are among this new generation of nanoparticles, consisting of a spherical dielectric core (generally polystyrene or silica) coated with a nanometer-thick layer of metal (usually silver or gold). The plasmonic resonances of nanoshells can be tuned from the visible to the infrared region of the spectrum by independently varying the composition and thickness of the metal layer, or the size and composition of the dielectric core.[6,14−18] Because of this tunability, nanoshells are a promising class of nanoparticles for SERS, offering the potential for strong enhancement over a wide range of excitation wavelengths.

SERS using metal nanoshells as substrates has been demonstrated both from their suspensions[8,19] and from nanoshells deposited on a solid support.[9,20,21] SERS of appropriate reporter molecules adsorbed on nanoshells has been employed for sensing biological molecules[11] and as nanoscale pH probes.[20,22] The SERS intensity from a monolayer of a nonresonant molecule adsorbed to a silica core−silver nanoshell substrate has been shown to be controlled by the nanoparticle geometry.[19] A study of the SERS response arising from Au and Ag nanoshells on glass slides as a function of nanoshell surface density indicated that the SERS intensity was mainly due to resonances arising from individual nanoshells,[9] meaning that no significant SERS enhancement was correlated to nanoshell dimers or aggregates. In addition, Talley et al.[13] reported that the SERS signals for isolated nanoshells and for dimers of adjacent nanoshells were similar. These results suggest that the surface roughness of individual nanoshells is sufficient to sustain SERS even in the absence of nanoshell aggregation, in contrast to the requirement for aggregation in systems of spherical metallic nanoparticles.[13] Recently, Rayleigh and surface-enhanced resonance Raman scattering (SERRS) from individual nanoshells in a flowing sample stream were monitored, showing the potential of "single-nanoshell" biosensing applications.[23] However, the variations in SERS efficiency between nanoshells were not explored in previous reports on the SERS of individual nanoshells.

In this work, we immobilized isolated silver nanoshells coated with dye molecules both on gold films and on silicon, and then we carried out SERRS mapping of individual nanoshells. Spectral variations, both frequency variations within a single nanoshell and also intensity variations between isolated nanoshells, were observed. The statistics of the resulting integrated SERRS intensity distributions were analyzed, showing similarities to the characteristic tailed statistics observed in single-molecule SERS. Specifically, we find that the distribution of integrated intensities between nanoshells follows Pareto-type behavior. These results indicate that a small number of nanoshells present SERS hotspots that are much more efficient than the average. This improved understanding of the statistics of nanoshell-to-nanoshell variation, arising from inherent heterogeneities both between and within nanoshells, is essential to future applications of single-nanoshell SERS.

Received: July 18, 2011
Revised: August 30, 2011
Published: August 30, 2011

ACS Publications © 2011 American Chemical Society

EXPERIMENTAL SECTION

Chemicals. Carboxylate-modified polystyrene (PS) latex beads with mean particle diameter of 400 nm, butylamine, silver nitrate, Nile blue A perchlorate, and 1,3-propanedithiol were purchased from Sigma−Aldrich and used as received. Gold films on glass slides (100 nm thick Au deposited on glass with 5 nm Cr adhesion layer) were obtained from Evaporated Metal Films Inc.

Preparation of Silver Nanoshells. Silver nanoshells were fabricated on carboxylate-modified PS latex beads according to a procedure previously described by Kim et al.[11] Briefly, an ethanolic suspension of PS beads (0.1 mg·mL^{-1}), $AgNO_3$ (1 mmol·L^{-1}), and butylamine (1 mmol·L^{-1}) were mixed and stirred for 50 min at 45 °C in a polypropylene tube. After that, the suspension was cooled to room temperature, centrifuged, and rinsed with ethanol.

The grayish suspension was incubated for 2 h with Nile blue (NB) at a final concentration of 80 μM. After the dye adsorption, the suspension was centrifuged and rinsed with ethanol three times in order to remove the remaining solubilized free dye. This final suspension was used for immobilizing silver nanoshells on the surfaces. The number of dye molecules per nanoshell can be estimated as ~2.5 × 10^6 molecules/nanoshell, considering that a monolayer of NB was formed (surface coverage of 8 × 10^{-10} mol·cm^{-2})[24] on a silver film coating the PS latex beads. The roughness of the silver surface provides a larger surface area, and the real value should be between 4 and 10 times larger than this estimate.

Glass slides coated with gold film were cleaned by 30 min of sonication in spectroscopic-grade acetone and methanol, successively, and then dried via a nitrogen flow. Then they were soaked in 50 mM 1,3-propanedithiol ethanolic solution for 24 h. The modified slides were rinsed with copious amounts of ethanol and immersed into the suspension of silver nanoshells with adsorbed dye overnight. Finally, the slides were rinsed again with ethanol and dried via a nitrogen stream.

Silicon wafer substrates were cleaned by immersion in a H_2SO_4/H_2O_2 (7/3 v/v) solution for 1 h, rinsed with deionized water, and dried via a nitrogen stream. The same procedure adopted for the immobilization of nanoshells on gold substrates was employed for the silicon wafers.

Instrumentation. The UV−vis extinction spectra were recorded on a Varian Cary 50 UV−vis spectrophotometer. Transmission electron microscopy (TEM) was performed on a Hitachi H-700 electron microscope, operating at an accelerating voltage of 70 kV.

Raman measurements were recorded on a Renishaw inVia Raman microscope system and a He−Ne laser source at 632.8 nm. The Raman mappings were recorded by use of a 100× objective (NA = 0.85) with a circular laser spot at the sample with a diameter (full width at half-maximuum, fwhm) equal to 500 nm. The step size used in the mappings was 500 nm in both directions of the plane of the slide. The mappings were built up by fitting a mixed Gaussian−Lorentzian curve to the NB band at ca. 590 cm^{-1} and measuring the peak intensity after background subtraction by use of the WiRE 3.1 software. It is important to emphasize that NB has an electronic transition centered at 630 nm and the SERS experiments were realized by use of the 632.8 nm excitation. Therefore, the resulting Raman intensities contain contributions from both resonance Raman and SERS. This type of double enhancement situation is described in the literature as "surface-enhanced *resonance* Raman scattering", or SERRS.

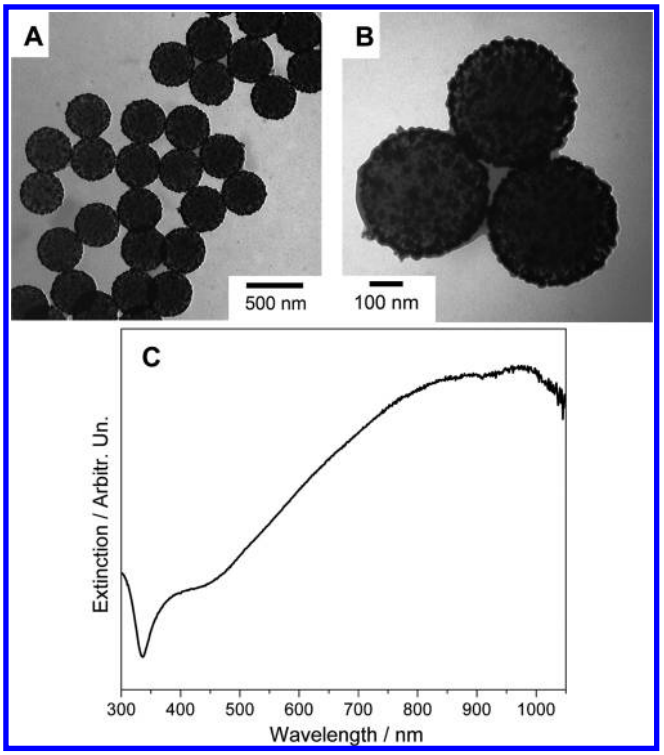

Figure 1. (A, B) Transmission electron microscopy (TEM) images of silver nanoshells grown on polystyrene latex spheres. (C) UV−vis absorption spectrum of silver nanoshells in ethanol suspension.

RESULTS AND DISCUSSION

Figure 1 shows typical transmission electron microscopy (TEM) images of silver nanoshells on polystyrene (PS) latex. The spherical shape and low polydispersity of the bare PS colloids are mostly preserved after nanoshell formation (Figure 1A). Higher-magnification TEM images of nanoshells (Figure 1B) reveal that the silver coatings are not continuous and consist of Ag nanoparticles of sizes ranging from 5 to 30 nm evenly covering the surfaces of the PS colloids.

The UV−vis absorption spectrum of the silver nanoshells (Figure 1C) shows a broad absorption band with maximum at ca. 900 nm. This spectrum is characteristic of metal nanoshells composed of coalesced silver nanoparticles on a PS core, in agreement with the TEM images.[17] The broad absorption band is a result of a distribution of morphologies for the silver nanoparticle aggregates on the PS spheres.[17]

Figure 2 presents the optical micrograph, scanning electron microscopy (SEM) image, and Raman mapping of a small number of NB-coated silver nanoshells immobilized on a thiol-modified gold film. The optical micrograph (Figure 2A) shows well-separated black spots on the micrometer scale, suggesting a low density of nanoshells on the gold surface. The nanoshell density on the surface was quantified by measuring the number of black spots in nine randomly selected regions of ca. 70 μm × 55 μm, giving a mean density of (1.2 ± 0.6) × 10^{-2} nanoshells·μm^{-2}. The large relative error (~50%) on the mean density, determined from the standard deviation of multiple measurements in different regions, reflects a low uniformity of the nanoshells adsorbed on the gold film. A SEM image of the same region of the sample (Figure 2C) confirms that the optically imaged diffraction-limited spots observed in Figure 2A are mainly due to single

dx.doi.org/10.1021/jp2068649 |J. Phys. Chem. C 2011, 115, 19104–19109

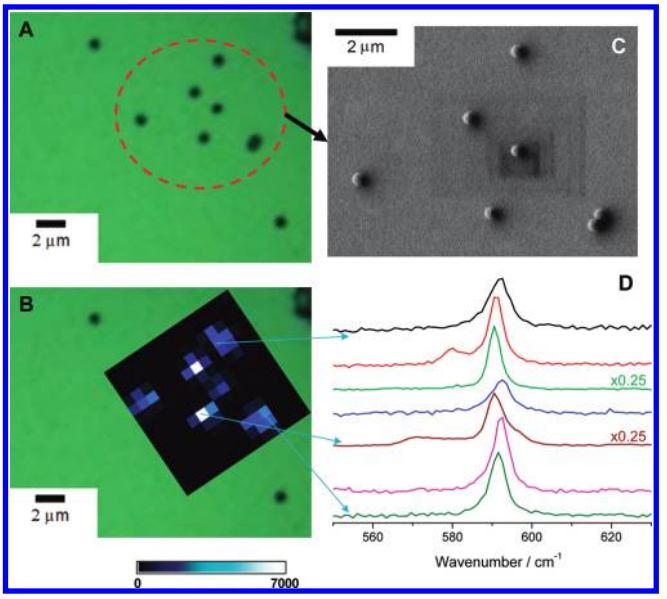

Figure 2. (A) Optical micrograph of nanoshells immobilized on a gold film. (B) Raman mapping monitoring the peak intensity of NB at ~590 cm^{-1}. (C) Scanning electron micrograph (SEM) of the same area shown in panel A. (D) Representative SERRS spectra of nanoshells shown in panel B.

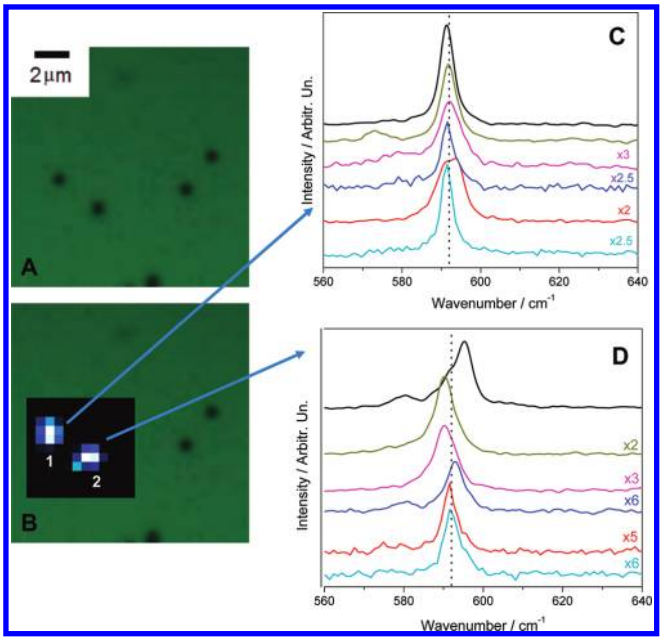

Figure 3. (A) Optical micrograph of nanoshells immobilized on a gold film. (B) Raman mapping monitoring the Nile blue peak intensity at ~590 cm^{-1}. (C, D) Representative SERRS spectra of nanoshells 1 and 2 mapped in panel B.

nanoshells, although one nanoshell dimer can be identified in the SEM picture. A careful examination of the optical micrograph in Figure 2A shows that the dark spot corresponding to the dimer of adjacent nanoshells is slightly larger and more elongated than those of single nanoshells, demonstrating that it is possible to distinguish single nanoshells from aggregates in optical micrographs.

As the nanoshells are relatively well-separated, it was possible to monitor the SERRS signal of individual nanoshells through Raman mapping. The Raman mapping was performed by monitoring the intensity of the ~590 cm^{-1} band (phenoxazine ring mode)[25] of NB, resulting in a clear correlation between the SERRS signal (Figure 2B) and optical image counterpart (Figure 2A). The most intense spectra from the mapping of each nanoshell in the designated region of Figure 2B are shown in Figure 2D. One notable feature in Figure 2D is the difference among SERRS spectra from different nanoshells, in terms of position, width, and intensity of the Raman peaks. In order to investigate these variations, SERRS spectra from different "regions" in the same nanoshell (mapping) were recorded for 177 nanoshells.

Figure 3 shows the mapping of a region containing two isolated nanoshells (designated nanoshells 1 and 2), along with selected SERRS spectra corresponding to different points of the Raman mapping on each nanoshell (Figure 3C, nanoshell 1; Figure 3D, nanoshell 2). Changes in width and frequency of the band at ca. 590 cm^{-1} are observed when the SERRS spectra from different regions of the SERRS mapping of a particular nanoshell are compared, with shifts up to 5 cm^{-1}. This type of spectral shape variation was previously reported for SERS of rhodamine 6G on isolated silver nanoparticles.[26] These observed shifts in spectra, either from the same nanoshell (Figure 3) or from different nanoshells (Figure 2), can be ascribed either to different adsorption sites or to differences in adsorption geometry.[26−28] In fact, the band at 590 cm^{-1} is assigned to the phenoxazine ring mode and is, therefore, expected to be sensitive to the adsorption geometry. It is well-known that the ring breathing modes of benzene, pyridine, and pyrazine shift to lower wavenumbers when the adsorbed molecule is oriented parallel to the surface, due to interaction between π electrons and the metal surface.[29,30] Therefore, the observed frequency variation in the NB spectra could be correlated to the orientation of the phenoxazine ring relative to the metal surface. The fact that these spectral differences are evident even within a single nanoshell highlights that a very small number of molecules is being probed at each mapped point.

Along with variations in peak position, we also observe differences in the SERS intensities of the ~590 cm^{-1} SERRS band at different mapping points, both within a given nanoshell and between different nanoshells. We observed that the variations in intensity are independent of changes in the other spectral parameters, such as the frequency of the ~590 cm^{-1} band and its full width at half-maximum. For instance, over the population of nanoshells, we did not observe a relationship between the position and the magnitude of the strongest SERS band for a given nanoshell.

Variations in the SERRS intensity from the nanoshells at different mapping points is expected for two reasons: (1) The first factor is the overlap between the incident laser spot (with a Gaussian intensity distribution) and the nanoshell during mapping. Since both the spot size and the nanoshell have similar dimensions (around 500 nm), the SERRS intensities recorded across a single nanoshell will have a magnitude that depends on the portion of the beam that overlaps with the nanoshell. In this case, the differences in relative intensities reflect the degree of overlap between the incident laser and the area being probed. (2) A second contribution would come from the different efficiencies of the hotspots across the surface of the nanoshell. Each nanoshell is composed of Ag nanostructures of different sizes, randomly aggregated on the PS surface (Figure 1). As a result, the nanoshells will contain specific regions that favor enhanced electric fields (hotspots) due to the excitation of localized surface

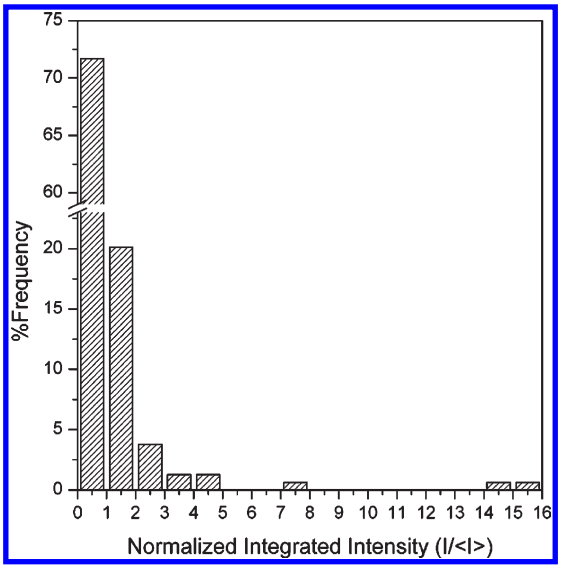

Figure 4. Histogram of integrated SERRS intensities normalized by the average of individual nanoshells (N = 177).

plasmons. This random distribution of hotspots that occurs across a particular nanoshell would also contribute to the intensity variations within a single nanoshell observed in the SERRS mapping.

Raman mapping from 177 individual nanoshells was recorded and analyzed to provide insights into the statistics of the nanoshell-to-nanoshell variations in SERRS intensity. Each map of a particular nanoshell contained at least nine spectra of various intensities in different regions. The area of the most intense band, at ~590 cm^{-1}, for each spectrum was calculated and summed over all regions, resulting in an integrated SERRS intensity for each nanoshell. Note that this procedure minimizes the effect of the laser beam−nanoshell overlap discussed above. The integrated SERRS intensities were then normalized by their average and plotted as a histogram in Figure 4. The shape for the distribution of SERRS intensities between nanoshells is skewed, showing a larger number of nanoshells with SERRS intensity below the average and a small number with SERRS intensity well above average. For instance, a few nanoshells present SERRS signal higher than 10 times the average value (Figure 4). The sampling was insufficient to allow a proper fitting of the experimental data to known statistics. However, we note that the shape of the histogram in Figure 4 presents an intriguing similarity to the distributions observed for single-molecule SERS experiments,[31,32] although our experiments were not done in the single-molecule regime.

In general, SERS measurements can be made in ensemble (a large number of molecules is probed) or in "single-molecule" conditions. SERS from colloidal suspensions with relatively high analyte concentrations (ensemble situation) is expected to present a normal (Gaussian) distribution of intensities, centered on the average value.[28,33] A log-normal intensity distribution, peaking below the average intensity and tailing for higher intensities, is generally reported as the condition for single-molecule SERS is approached.[32,33] Such a skewed distribution shape reflects both the statistics of rare events and the dominant contribution of a small number of highly enhancing hotspots to the observed intensity. As the number of molecules within the laser beam becomes small relative to the number of hotspots, the probability of probing a molecule on a hotspot also diminishes. Moreover, minute variations in the location of an adsorbed molecule within the most-enhancing hotspots lead to large fluctuations in the measured intensity. As a result, only a relatively small number of spectra, corresponding to molecules adsorbed closest to the region of strongest field enhancement, present intensities well above the average value.

In the present case, the observed distribution of SERRS intensities for single nanoshells, shown in Figure 4, is similar to those obtained in the single-molecule SERS condition, even though our experiments were not done under true single-molecule conditions. A relatively high concentration of dye was employed in our experiments in order to completely cover the silver surface with NB molecules (~2.5×10^6 molecules/nanoshell was estimated, without consideration of the roughness of the silver clusters). On the other hand, nanoshell surfaces consist of aggregated Ag nanoparticles of different sizes with no particular order or arrangement. The PS beads act as a support for these nanoparticles, and when these aggregates assume a specific configuration by chance (for instance, a junction between the Ag clusters is formed), a hotspot is produced. The distribution of SERRS intensities for single nanoshells suggests that the efficiency of the hotspots varies from nanoshell to nanoshell, due to this random formation of silver aggregates at their surface; hence, only a very small fraction of the nanoshells presents hotspots that yield enhancements larger than an average value. As a result, a tailed intensity distribution analogous to that observed in single-molecule SERS is obtained, although a molecular ensemble is probed in the single-nanoshell case reported here.

The results presented so far are for silver nanoshells immobilized on gold films. The advantage of using gold films as supporting substrates is that their conductivity makes it easier to obtain high-quality SEM images. However, surface plasmons can potentially be excited on thin gold films, and the junction between the nanoshell and the metal may also constitute an electromagnetic hotspot. In fact, recent work has demonstrated the coupling between the localized surface plasmon of spherical metallic nanoparticles and the surface plasmon from a gold film substrate. This coupling can increase the SERS efficiency at that particular location and could potentially have an effect on the observed statistics.[34,35] In order to verify the generality of the nanoshell statistics indicated in Figures 2−4, a new set of experiments was performed where nanoshells from the same batch were divided and immobilized on both a gold film and a silicon wafer. The same conditions for Raman measurements of NB were applied to both samples. For the nanoshells deposited on the Si substrate, variations in the SERRS intensities and position of the ~590 cm^{-1} SERRS band were observed at different mapping points, both within a given nanoshell and between different nanoshells, exactly as observed on the Au substrate. Additionally, the histograms of the integrated and normalized SERRS intensities of nanoshells (from the same batch) immobilized on either Au or Si substrates present similar skewed shapes, as shown in Figure 5. However, the mean SERRS intensity observed for the nanoshells immobilized on Au is ca. 3 times higher than that observed for nanoshells on Si (not shown). This modest SERS increase indicates some coupling between the localized surface plasmons of the Ag nanoshells and the gold film, but this coupling does not lead to a significant modification of the overall SERS enhancement intensity, as previously observed for Au nanoparticles.[34,35] The profile of SERRS intensity histograms (nanoshell-to-nanoshell variation) are very similar for the two substrates (Figure 5), suggesting that the intensity distribution is

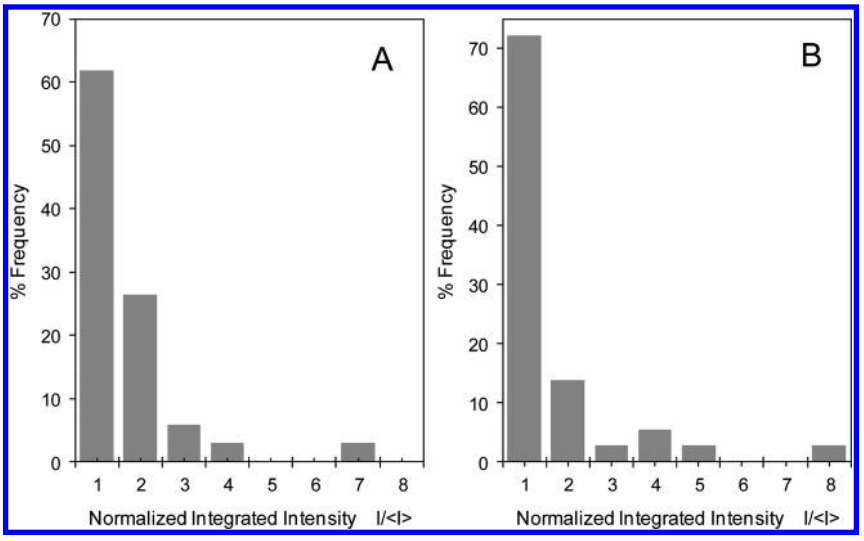

Figure 5. Histograms of integrated SERRS intensities normalized by the average of individual nanoshells ($N = 35$) immobilized on (A) Au film and (B) Si wafer.

a characteristic property of the nanoshells irrespective of the substrate.

CONCLUSIONS

In summary, this report describes variations in the position and intensity of the SERRS signal from NB on individual silver nanoshells immobilized on gold films and silicon. We observed variations in spectral shape (width and frequency) and intensity for different mapping points within a single nanoshell and between different nanoshells within the ensemble. The frequency differences were assigned to different adsorption sites or molecular adsorption geometries. The histograms representing the SERRS intensity distributions for different nanoshells present a skewed shape with a long tail that resembles the statistics for single-molecule SERS. This is understood by considering that the SERRS signal from a small number of nanoshells presents highly efficient hotspots formed by chance as silver nanoparticles cluster on the nanoshell surface. These results indicate a degree of variability for the SERRS intensity from nanoshells coated with a random distribution of metal nanoparticles. This work then indicates that although single nanoshells provide several advantages for applications in chemical sensing and SERS imaging, particle-to-particle spectral variability must be carefully evaluated and taken into consideration for single-particle applications.

AUTHOR INFORMATION

Corresponding Author

*E-mail agbrolo@uvic.ca.

ACKNOWLEDGMENT

We gratefully acknowledge the Natural Science and Engineering Research Council of Canada (NSERC). C.M.S.I. is grateful for a scholarship provided by the Brazilian agency CAPES (3113-08-6).

REFERENCES

(1) Aroca, R. *Surface-Enhanced Vibrational Spectroscopy*; John Wiley & Sons, Ltd.: New York, 2006.
(2) Le Ru, E. C.; Etchegoin, P. G. *Principles of Surface-Enhanced Raman Spectroscopy*; Elsevier: New York, 2009.
(3) Campion, A.; Kambhampati, P. *Chem. Soc. Rev.* **1998**, *27*, 241.
(4) Cui, B.; Clime, L.; Li, K.; Veres, T. *Nanotechnology* **2008**, *19*, No. 145302.
(5) Tiwari, V. S.; Oleg, T.; Darbha, G. K.; Hardy, W.; Singh, J. P.; Ray, P. C. *Chem. Phys. Lett.* **2007**, *446*, 77.
(6) Levin, C. S.; Kundu, J.; Barhoumi, A.; Halas, N. J. *Analyst* **2009**, *134*, 1745.
(7) Allgeyer, E. S.; Pongan, A.; Browne, M.; Mason, M. D. *Nano Lett.* **2009**, *9*, 3816.
(8) Oldenburg, S. J.; Westcott, S. L.; Averitt, R. D.; Halas, N. J. *J. Chem. Phys.* **1999**, *111*, 4729.
(9) Jackson, J. B.; Halas, N. J. *Proc. Natl. Acad. Sci. U.S.A.* **2004**, *101*, 17930.
(10) Lal, S.; Grady, N. K.; Kundu, J.; Levin, C. S.; Lassiter, J. B.; Halas, N. J. *Chem. Soc. Rev.* **2008**, *37*, 898.
(11) Kim, K.; Lee, H. B.; Park, H. K.; Shin, K. S. *J. Colloid Interface Sci.* **2008**, *318*, 195.
(12) Jensen, R. A.; Sherin, J.; Emory, S. R. *Appl. Spectrosc.* **2007**, *61*, 832.
(13) Talley, C. E.; Jackson, J. B.; Oubre, C.; Grady, N. K.; Hollars, C. W.; Lane, S. M.; Huser, T. R.; Nordlander, P.; Halas, N. J. *Nano Lett.* **2005**, *5*, 1569.
(14) Oldenburg, S. J.; Averitt, R. D.; Westcott, S. L.; Halas, N. J. *Chem. Phys. Lett.* **1998**, *288*, 243.
(15) Jackson, J. B.; Halas, N. J. *J. Phys. Chem. B* **2001**, *105*, 2743.
(16) Prodan, E.; Nordlander, P. *Nano Lett.* **2003**, *3*, 543.
(17) Yong, K.-T.; Sahoo, Y.; Swihart, M. T.; Prasad, P. N. *Colloids Surf., A* **2006**, *290*, 89.
(18) Shi, W. L.; Sahoo, Y.; Swihart, M. T.; Prasad, P. N. *Langmuir* **2005**, *21*, 1610.
(19) Jackson, J. B.; Westcott, S. L.; Hirsch, L. R.; West, J. L.; Halas, N. J. *Appl. Phys. Lett.* **2003**, *82*, 257.
(20) Bishnoi, S. W.; Rozell, C. J.; Levin, C. S.; Gheith, M. K.; Johnson, B. R.; Johnson, D. H.; Halas, N. J. *Nano Lett.* **2006**, *6*, 1687.
(21) Wei, F.; Zhang, D. M.; Halas, N. J.; Hartgerink, J. D. *J. Phys. Chem. B* **2008**, *112*, 9158.
(22) Jensen, R. A.; Sherin, J.; Emory, S. R. *Appl. Spectrosc.* **2007**, *61*, 832.
(23) Sebba, D. S.; Watson, D. A.; Nolan, J. P. *ACS Nano* **2009**, *3*, 1477.
(24) Brolo, A. G.; Sanderson, A. C. *Can. J. Chem.—Rev. Can. Chim.* **2004**, *82*, 1474.
(25) Lawless, M. K.; Mathies, R. A. *J. Chem. Phys.* **1992**, *96*, 8037.
(26) Nie, S.; Emory, S. R. *Science* **1997**, *275*, 1102.

(27) Qian, X. M.; Nie, S. M. *Chem. Soc. Rev.* **2008**, *37*, 912.
(28) Pieczonka, N. P. W.; Aroca, R. F. *ChemPhysChem* **2005**, *6*, 2473.
(29) Brolo, A. G.; Irish, D. E. *J. Electroanal. Chem.* **1996**, *414*, 183.
(30) Haq, S.; King, D. A. *J. Phys. Chem.* **1996**, *100*, 16957.
(31) Le Ru, E. C.; Meyer, M.; Etchegoin, P. G. *J. Phys. Chem. B* **2006**, *110*, 1944.
(32) Etchegoin, P. G.; Meyer, M.; Blackie, E.; Le Ru, E. C. *Anal. Chem.* **2007**, *79*, 8411.
(33) dos Santos, D. P.; Andrade, G. F. S.; Temperini, M. L. A.; Brolo, A. G. *J. Phys. Chem. C* **2009**, *113*, 17737.
(34) Sisco, P. N.; Murphy, C. J. *J. Phys. Chem. A* **2009**, *113*, 3973.
(35) Hill, R. T.; Mock, J. J.; Urzhumov, Y.; Sebba, D. S.; Oldenburg, S. J.; Chen, S.-Y.; Lazarides, A. A.; Chilkoti, A.; Smith, D. R. *Nano Lett.* **2010**, *10*, 4150.